JACS
JOURNAL OF THE AMERICAN CHEMICAL SOCIETY
Article
pubs.acs.org/JACS

Dissociative Photoionization of Glycerol and its Dimer Occurs Predominantly via a Ternary Hydrogen-Bridged Ion−Molecule Complex

Franziska Bell,[†,‡,∥] Qiao N. Ruan,[†,‡,∥] Amir Golan,[†,‡,§] Paul R. Horn,[†,‡] Musahid Ahmed,[‡] Stephen R. Leone,[†,‡,§] and Martin Head-Gordon*[,†,‡]

[†]Department of Chemistry and [§]Department of Physics, University of California, Berkeley, California 94720, United States
[‡]Chemical Sciences Division, Lawrence Berkeley National Laboratory, Berkeley, California 94720, United States

Supporting Information

ABSTRACT: The photoionization and dissociative photoionization of glycerol are studied experimentally and theoretically. Time-of-flight mass spectrometry combined with vacuum ultraviolet synchrotron radiation ranging from 8 to 15 eV is used to investigate the nature of the major fragments and their corresponding appearance energies. Deuterium (1,1,2,3,3-D5) and ^{13}C (2-^{13}C) labeling is employed to narrow down the possible dissociation mechanisms leading to the major fragment ions ($C_3H_xO_2^+$, $C_2H_xO_2^+$, $C_2H_xO^+$, CH_xO^+). We find that the primary fragmentation of the glycerol radical cation (m/z 92) occurs only via two routes. The first channel proceeds via a six-membered hydrogen-transfer transition state, leading to a common stable ternary intermediate, comprised of neutral water, neutral formaldehyde, and a vinyl alcohol radical cation, which exhibits a binding energy of ≈42 kcal/mol and a very short (1.4 Å) hydrogen bond. Fragmentation of this intermediate gives rise to experimentally observed m/z 74, 62, 44, and 45. Fragments m/z 74 and 62 both consist of hydrogen-bridged ion−molecule complexes with binding energy >25 kcal/mol, whereas the m/z 44 species lacks such stabilization. This explains why water- or formaldehyde-loss products are observed first. The second primary fragmentation route arises from cleaving the elongated C−C bond. Also for this channel, intermediates comprised of hydrogen-bridged ion−molecule complexes exhibiting binding energies >24 kcal/mol are observed. Energy decomposition analysis reveals that electrostatic and charge-transfer interactions are equally important in hydrogen-bridged ion−molecule complexes. Furthermore, the dissociative photoionization of the glycerol dimer is investigated and compared to the main pathways for the monomeric species. To a first approximation, the glycerol dimer radical cation can be described as a monomeric glycerol radical cation in the presence of a spectator glycerol, thus giving rise to a dissociation pattern similar to that of the monomer.

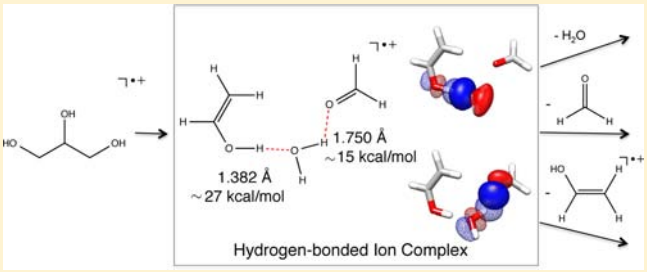

1. INTRODUCTION

Glycerol (propane-1,2,3-triol) is widely present in nature as an intermediate in many biological pathways,[1] is ubiquitous in pharmaceutical formulations,[2] and furthermore is used as a model system to understand sugar chemistry. Carbohydrates are a major biomass constituent, playing an important role in biology[2] and energy science.[3,4] In particular, the potential of using carbohydrates as biofuels[5] makes their pathways an intensively studied subject.[6−8] The three adjacent hydroxyl groups in glycerol resemble features of the much more complex structure of carbohydrates and their polymeric forms, such as cellulose, and so it is considered a simple model for complex carbohydrates.

So far, both theoretical and experimental work has been aimed at elucidating the pathways involved in the pyrolysis of glycerol,[9−15] with particular focus on the dehydration mechanisms.[11−13] Loss of one or two water molecules in glycerol is facile under these conditions. However due to the presence of three hydroxyl groups on a relatively flexible carbon backbone, many different pathways are possible.[10−13] Since a detailed mechanistic experimental study of glycerol pyrolysis has yet to be carried out, there has been considerable debate in the literature.[9,10]

In particular, more evidence based on real-time analysis and isomeric selectivity is needed to fully understand the pyrolysis mechanism of glycerol. This may be obtained by using synchrotron vacuum ultraviolet (VUV) photoionization, coupled with time-of-flight mass spectrometry (TOF-MS). This approach features several advantages. First, the molecular-beam reduces collision effects and allows unstable intermediates to be isolated. Furthermore, the high-energy resolution and tunability of the synchrotron light source minimizes fragmentation and allows different isomers to be distinguished.[16−18] Indeed, recent pyrolytic experiments employing synchrotron VUV photoionization at low pressure, coupled with TOF-MS

Received: June 2, 2013
Published: August 7, 2013

dx.doi.org/10.1021/ja405511v | J. Am. Chem. Soc. 2013, 135, 14229−14239

have given new insights into other combustion mechanisms.[19−21]

However, in order to interpret VUV-TOF-MS data, untangling channels due to pyrolysis from those due to photoionization is necessary. To our knowledge, detailed studies of dissociative photoionization of glycerol in the VUV region are not yet available, and thus such a study may form the basis of resolving the ongoing debate in the literature.[9,10]

Motivated by this, we investigate the dissociative photoionization of glycerol using synchrotron radiation between 8 and 15 eV. Photoionization efficiency (PIE) curves of the major fragment ions are used to evaluate the corresponding appearance energies (AEs) resulting from the dissociative photoionization. The possible reaction channels for the major fragments are narrowed down using isotopically labeled samples (1,1,2,3,3-D5 and 2-^{13}C glycerol, respectively). Wave function and density functional based calculations are carried out to characterize the lowest conformers on the radical cation surface and to further distinguish between the possible reaction pathways. Furthermore, the dissociative photoionization of the gas-phase glycerol dimer is investigated and compared to the proposed pathways for the monomeric species. Understanding its fragmentation pathways forms the first step in a series of investigations involving increasingly complex polyol compounds in order to elucidate the mechanisms involved in carbohydrate chemistry.

We find hydrogen-bridged ion−molecule complexes (essentially very strong hydrogen bonding, driven by better accommodating the net charge) to be a recurring theme and crucial feature in understanding the photodissociation pathways of glycerol. In particular, this interaction causes the experimentally observed appearance energies for several key fragments to be due to the barrier affiliated with the separation of the products rather than the preceding rearrangement reactions. Furthermore, several product fragments are found to feature hydrogen-bridged ion−molecule interactions, which allow for charge and spin delocalization between fragments. Hydrogen-bridged ion−molecule interactions are found to typically lie between 5 and 35 kcal/mol[22] and are proposed to play a key role in biology and chemistry, such as protein folding, enzyme activity,[23,24] biomolecular recognition and sensors,[25] surface adsorption, self-assembly in supramolecular chemistry and molecular crystals,[26−29] electrolytes, ion solvation,[30] and ionic clusters.[31−33] In the context of ionic rearrangements in low-energy radical species, hydrogen-bridged radical cations, in particular those containing a O···H···O or N···H···O moiety, have been proposed to form stable intermediates.[34−37] Moreover, such observations have not been limited to the gas phase. For example, a hydrogen-bridged ion has been proposed to play a key role in the B_{12}-catalyzed dehydration reaction of ethylene glycol.[38] Despite the apparent importance of such hydrogen-bond mediated ion−molecule interactions, the nature of their bonding is only poorly understood. In the past, the interaction was attributed to ion−dipole interactions.[39] However, using energy decomposition analysis (EDA),[40] we are able to quantify the various components in hydrogen-bridged ion−molecule complexes and find that charge-transfer interactions are equally as important as permanent and induced electrostatic effects.

2. METHODS

2.1. Experimental Section. Experiments are performed on a supersonic molecular beam and an effusive beam setup coupled with VUV monochromatic radiation. The ionizing VUV radiation is provided by a 10 cm period undulator of the Chemical Dynamics Beamline at the Advanced Light Source, Lawrence Berkeley National Laboratory. The radiation is quasi-continuous (70 ps pulses at 500 MHz). Higher harmonics are filtered out by passing the radiation through an argon gas filter. The monochromatized light is obtained via a 3 m monochromator with an average flux of 10^{13} photons per second. Details of the molecular beam apparatus have been described elsewhere.[41−43]

In the experiment, 50 mg of liquid glycerol (99% purity, Sigma Aldrich) without further purification are introduced into a 3/8 in. stainless steel cylindrical nozzle with a 100 μm diameter orifice. The nozzle is heated to 105 or 185 °C using a cartridge heater to create sufficient vapor pressure in 50 kPa (150 Torr) of argon before the expansion into vacuum. The beam consisting of neutral monomeric glycerol as well as clusters then passes through a 2 mm diameter skimmer before it reaches the photoionization region. The skimmed molecular beam is interrogated by the VUV radiation in the ionization region of a TOF reflectron mass spectrometer, where 1200 V across ∼1 cm are applied. If any Rydberg states should be populated, they would field ionize under these conditions and yield characteristic peaks in the PIE curve at energies below the adiabatic ionization energy. However, no such signature is observed, and thus their presence can be excluded.

To avoid cluster formation, we use an alternative, effusive source to introduce the sample into the photoionization region. The effusive beam is generated by thermally vaporizing the sample in an oven attached to the repeller plate of the ion optics. The vapors then pass through a 1 mm orifice in the plate which is located ∼1 cm below the interaction region. In this case, the experiment is carried out under ambient temperatures.

The step size of the VUV photon energy in these experiments is 0.10 eV, and the data collection time at each step is 240 s. The PIE curves are obtained by integrating over the mass peaks at each photon energy and normalizing by the photon flux measured by a photodiode.

Unlabeled glycerol is obtained from Sigma-Aldrich, whereas the two isotopologue samples, 1,1,2,3,3-D5 glycerol and 2-^{13}C glycerol are from Cambridge Isotope Laboratories, Inc. All glycerol isotopologue samples are nominally 99% isotopically pure and used without further purification.

2.2. Computational. Calculations are carried out using a developer's version of Q-Chem 3.2.[44]

2.2.1. Radical Conformers. Structures of neutral glycerol given in a recent study[14] are used as a starting point in the geometry optimizations of the radical cation conformers. In order to obtain a quantitative distribution of glycerol conformers, structures are optimized using the Becke, three-parameter, Lee−Yang−Parr exchange correlation functional, B3LYP/6-311++G(p,d),[45] and Møller-Plesset perturbation theory to second order,[46] MP2/6-311++G(p,d). A few conformers indicate considerable changes in geometry upon reoptimization with MP2, a possible indicator for a shallow potential energy surface. Frequency calculations are carried out on all species to confirm local minima. Relative energies are calculated with B3LYP and the range-separated hybrid functional ωB97X[47] with the 6-311++G(2df,2pd) basis and MP2/aug-cc-pVTZ. For the conformers lowest in energy, the complete basis set (CBS) limit is approximated by extrapolation to the MP2/aug-cc-pV(TQ)Z level by using[48]

$$E_{XY} = E_{\mathrm{SCF},Y} + \frac{X^3 E_{\mathrm{corr},X} - Y^3 E_{\mathrm{corr},Y}}{X^3 - Y^3};\ Y > X \qquad (1)$$

where $X = 3$ and $Y = 4$ for the $T \rightarrow Q$ extrapolation. Spin contamination is very low for the radical cation conformers ($\langle S^2\rangle_{(\mathrm{B3LYP},\ \omega\mathrm{B97X})} \approx 0.753$, $\langle S^2\rangle_{(\mathrm{HF})} \approx 0.775$).

2.2.2. Ionization Energies. Vertical and adiabatic ionization energies are obtained at different levels of theory, including B3LYP, ωB97X, MP2, and coupled-cluster singles and doubles with perturbative triples correction, (U)CCSD(T),[49,50] with various different basis sets. Details can be found in Tables S2 and S3. No frequency corrections are carried out since the adiabatic and vertical geometries are substantially

different on the radical cation surface, and thus harmonic frequency corrections will yield considerable errors.

2.2.3. Transition States. Guesses for the transition-state structures are obtained using the freezing string method[51] (B3LYP/6-31G(d)), which requires reactant and product structures as input (unless otherwise indicated, radical cation conformer 100 is used as reactant). Using these guesses, transition states are then located at the level of B3LYP/6-31+G(p,d) and ωB97X/6-31+G(p,d). Frequency calculations confirm that they lie at a first-order saddle point.

The effect of basis set is studied for both B3LYP and ωB97X, by carrying out single point calculations with the considerably larger 6-311++G(2df,p) basis set, and the energy variation is found to be 0.19 eV, at the most (Table S6). Furthermore, single point calculations using UCCSD(T)/6-31+G(p,d) are carried out using the frozen core approximation. Finally, transition-state structures are followed by intrinsic reaction coordinate calculations (IRC)[52] in mass-weighted coordinates toward reactants and products.

2.2.4. Choice of Functional. The well-known self-interaction problem[53] may lead to errors in energies and bond lengths when using the still widely popular B3LYP functional. Although self-interaction is not fully resolved in ωB97X,[54] it is known to vastly improve upon B3LYP and has recently been shown to yield an ∼2.5 smaller average mean unsigned deviation in transition-state geometries when tested on the TSG48 set which involves geometrical data on 48 transition states.[55]

2.2.5. Glycerol Dimer. Glycerol dimer conformers are obtained by performing a molecular mechanics conformer search in Spartan[56] using the Merck molecular force field (MMFF)[57] in combination with three Monte Carlo runs, each starting from different points and each of which are terminated after 2000 steps. In the simulation, 100 conformers are retained. Finally the lowest 50 conformers are selected and reoptimized using B3LYP/6-311++G(p,d).

3. RESULTS AND DISCUSSION

3.1. Experimental Measurements. Figure 1a shows the photoionization mass spectrum of glycerol at 10.5 eV in a supersonic beam. The major fragment ions are at m/z 44, 45, 60, 61, 62, and 74. Due to the energetic preference of forming intermolecular rather than intramolecular hydrogen bonds in glycerol, extensive cluster formation occurs in the supersonic expansion process, and ion clusters of various sizes are observed in the mass spectrum. However, no ion clusters are detected under effusive conditions (Figure 1b) as a result of the low likelihood of forming glycerol dimers (or higher order clusters) in the vaporization process. The parent signal (m/z 92) is of very low intensity compared to the lower m/z fragment ions.

Figure 1c shows the dissociative photoionization mass spectrum of D5 glycerol using the effusive beam method and a photon energy of 10.5 eV. As expected, the mass spectra of 2-^{13}C-glycerol (Figure 1d) are very similar to the ones derived from unlabeled glycerol (Figure 1b) except that almost every peak is shifted 1 amu higher due to one extra neutron in ^{13}C.

Figure 2 shows the PIE curves of (a) the parent ion $C_3H_8O_3^+$ (m/z 92) and the major fragment ions $C_3H_6O_2^+$ (m/z 74), $C_2H_6O_2^+$ (m/z 62), $C_2H_4O^+$(m/z 44) (b–d, respectively). The PIE curves obtained from the supersonic expansion molecular beam and effusive molecular source for a particular fragment ion are rescaled to fit on the same figure for comparison (Figure 2).

The AE for each PIE curve can be determined by using a linear least-squares fit in the threshold region[58,59] and are listed in Table 2. The similarity of the PIE curves and corresponding AEs for both types of molecular beams indicates that the photofragment ions with m/z < 92 originate from monomeric glycerol in both experimental settings.

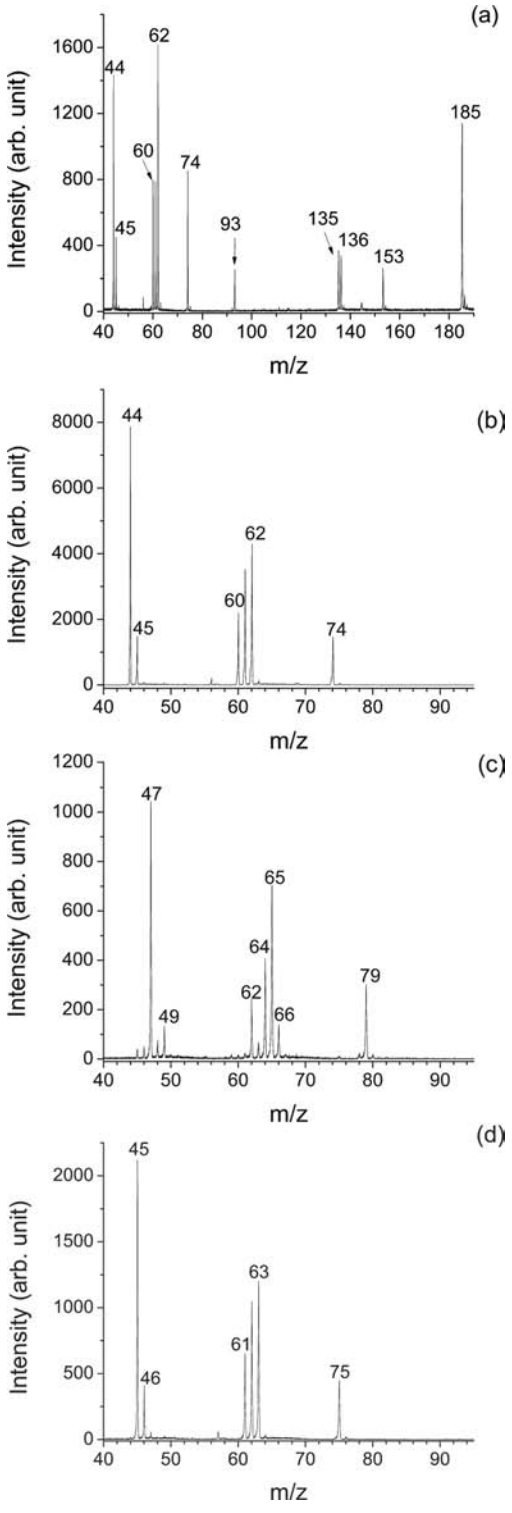

Figure 1. Photoionization TOF mass spectrum of glycerol at 10.5 eV in (a) supersonic expansion, (b) effusive source, (c) D5-glycerol, and (d) 2-^{13}C-glycerol in an effusive source.

The experimental breakdown diagram is generated by plotting the relative abundance of each fragment ion against photon energy with the sum of the abundance normalized to 1. The breakdown curves corresponding to the dissociation of glycerol are plotted in Figure 3, where only the major fragments are shown for clarity. The fractional abundance of ion m/z 92 decreases while that of fragment ions m/z 74, 62, and 60 rises.

dx.doi.org/10.1021/ja405511v | J. Am. Chem. Soc. 2013, 135, 14229–14239

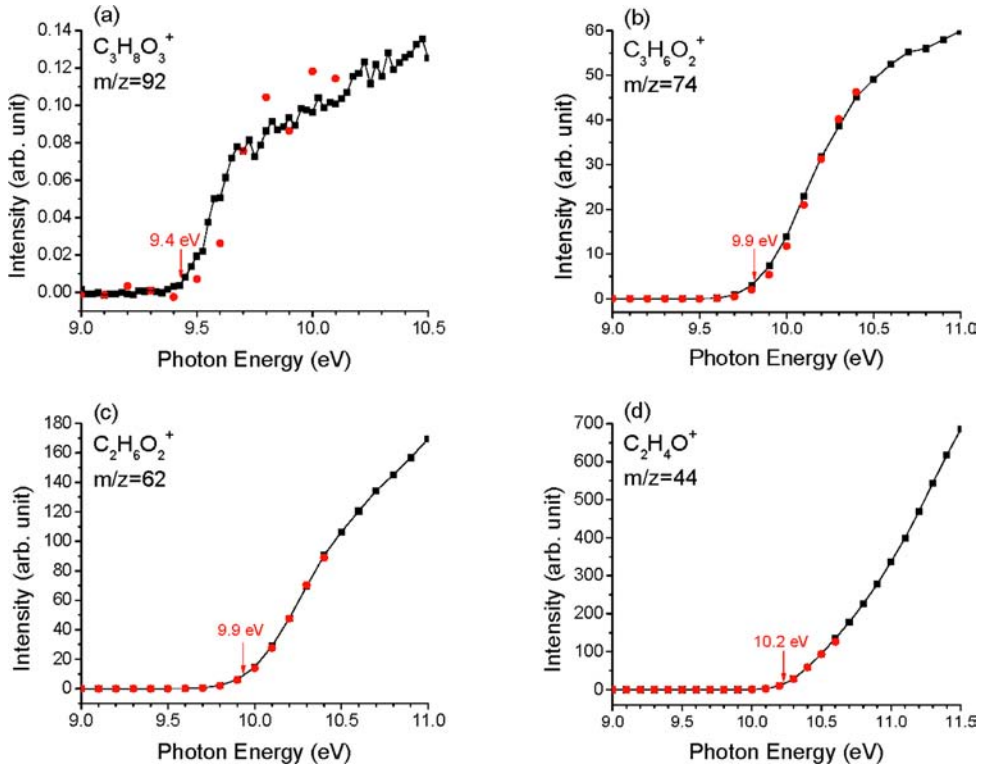

Figure 2. (a) Normalized PIE curves for the parent ion $C_3H_8O_3^+$. The adiabatic IE is found to be 9.4 ± 0.1 eV (supersonic expansion). (b–d) Normalized PIE curves for $C_3H_6O_2^+$, $C_2H_6O_2^+$, and $C_2H_4O^+$, respectively. Red circles: supersonic expansion, black rectangles: effusive conditions. AEs shown are from the supersonic expansion.

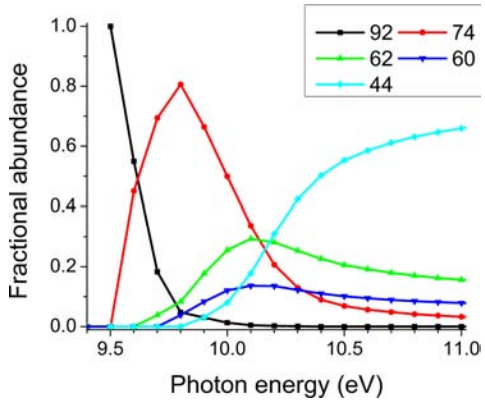

Figure 3. Overall breakdown diagrams for glycerol in the 9.4–11.0 eV photon energy region. The major fragments *m*/*z* 92, 74, 62, 60, and 44 are shown.

This implies that the smaller fragments *m*/*z* 74, 62, and 60 derive from the parent fragment *m*/*z* 92. Similar analysis for fragments *m*/*z* 44 and 45 indicates that these species may originate from *m*/*z* 92 or 74 or even both. Moreover the sum of the fractional abundance of *m*/*z* 74, 62, and 44 consistently represents around 85% of the total amount of fragment ions over this energy range. This suggests a common intermediate is produced first, which on dissociation (via different pathways) yields the three fragment ions of *m*/*z* 74, 62, and 44.

3.2. Monomeric Glycerol. *3.2.1. Radical Conformers.* An extensive conformer search of neutral glycerol has been carried out previously.[14] For both supersonic and effusive beam experiments, only two neutral conformers (labeled 100 and 95 in the previous study and shown in Figure 4) are thermally accessible.

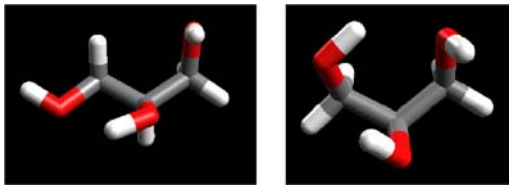

Figure 4. The energetically two lowest neutral gas-phase conformers. Left: conformer 95, right: conformer 100. C: gray, O: red, H: white.

The calculated adiabatic ionization energies for conformers 100 and 95 (9.34 and 9.57 eV, CCSD(T)/aug-cc-pVDZ//B3LYP/6-311++G(p,d)) are in good agreement with the experimentally observed value, which was found to be 9.4 ± 0.1 eV under supersonic conditions. Computed vertical ionization energies for various different density functionals and wave function based methods and basis sets all lie within a similar range (10.16–10.33 eV, Table S2).

The vertical ionization energies of conformer 100 and 95 lie at 0.86 and 0.93 eV above the corresponding adiabatic transition, respectively (CCSD(T)/aug-cc-pVDZ//B3LYP/6-311++G(p,d)). This leaves the molecule, once ionized, in a vibrationally and rotationally excited state. Due to the presence of this excess energy upon vertical excitation, interconversion between different conformers on the radical cation surface will be facile. Therefore, although the experimental temperature (especially in the supersonic beam experiment) is rather low, most of the conformational surface will be accessible to the

dx.doi.org/10.1021/ja405511v | J. Am. Chem. Soc. 2013, 135, 14229–14239

radical cation. The results of an extensive conformational search on the radical cation surface are given in the Tables S4 and S5.

Despite the vast number of possible conformers, they are found to fall into only six subgroups, which are based on their geometrical parameters, such as relative C−C bond lengths and the presence of hydrogen bonds. Geometrical parameters and relative energies of representatives of each of these main subclasses are given in Table 1, along with the 10 lowest-lying

Table 1. Structural Features and Relative Energies (single points, kcal/mol) of Representative Gas-Phase Monomeric Glycerol Radical Cation Conformers (conf) for Each of the Subclasses as well as the 10 Lowest Conformers[a]

	structural features				rel. energies	
	B3LYP 6-311++G(p,d)					
conf	O···H (Å)	CT/TT	C−C long (Å)	C−C short (Å)	MP2/aug-cc-pVTZ	MP2/T→Q extrap.
75	1.985	TT	1.94	1.51	0.33	
18	2.05	TT	2.01	1.51	2.30	
57	3.11	TT	1.62	1.62	8.18	
100	1.925	CT	1.90	1.51	0.00	0.00
109	1.981	CT	1.96	1.51	−0.57	−0.40
48	1.977	CT	1.96	1.51	−0.60	−1.03
43	1.985	CT	1.96	1.51	−0.58	−0.94
2	1.985	CT	1.96	1.51	−0.58	−0.94
34	1.994	CT	1.98	1.51	−0.68	−1.12
66	1.989	CT	1.98	1.50	−0.68	−1.12
80	1.993	CT	1.98	1.51	−0.71	−1.13
67	1.989	CT	1.98	1.51	−0.68	−1.12
116	3.08	CT	1.95	1.51	2.49	
9	2.60	CT	1.63	1.63	9.41	

[a]O···H lists the shortest hydrogen bond. CT/TT indicates whether the shortest hydrogen bond occurs between a central and a terminal (CT) or two terminal (TT) OH-groups.

conformers. Contrary to chemical intuition, which would predict ionization to occur primarily from the lone pair on the oxygen atoms, all low-lying relaxed radical cation conformers have an extended C−C bond length compared to neutral glycerol. Depending on the conformer under consideration, the extended C−C bond length lies between 1.61 and 2.02 Å (Table S4), which is in agreement with previous studies reported on oxygen containing radical cations.[60−63] This behavior was studied in detail for the ethane radical cation,[64] and similarly to this case we expect interconversion between the various conformers to be facile, resulting in the energetically lowest-lying conformers to actually collapse to one thermally averaged structure.

In order to rule out any channels that may proceed via an electronically excited state of the radical cation, a time-dependent density functional theory (TD-DFT, ωB97X/6-311++G(p,d)) calculation was carried out on the vertically ionized glycerol geometry of conformer 100. The lowest optically allowed excitation lies at 10.98 eV with respect to neutral conformer 100.

3.2.2. Fragmentation Pathways. Figure 5 summarizes the dominant photofragmentation pathways of monomeric glycerol that we find to be consistent with our computations and experimental data. Although many different mechanisms (see Supporting Information) could give rise to the fragments shown in Figure 5, we find that primary fragmentation of the glycerol radical cation occurs only via two routes.

The first route involves a low-lying (0.38 eV, Table 2) six-membered proton-transfer transition state (**TS1**, Figure 5), which is promoted by hydrogen bonding between the two terminal OH groups and the weakened C−C framework caused by ionization. **TS1** leads to a ternary hydrogen-bridged ion−molecule intermediate (**COM1**), comprised of water, formaldehyde, and vinyl alcohol radical cation. Fragmentation of this intermediate is found to be responsible for water loss (m/z 74, **COM2**), formaldehyde loss (m/z 62, **COM3**), vinyl alcohol radical cation formation (m/z 44, **P4**), and potentially also formation of fragment ion m/z 45. Although six-membered transition states are commonly proposed in organic reactions, and for neutral glycerol formation of the vinyl alcohol via such an arrangement was indeed predicted,[11] an intermediate complex composed of two neutral species and a radical cation, such as **COM1**, has not been previously considered in the literature. As will be discussed in the next section, the vinyl alcohol radical cation forms a hydrogen-bridged ion−molecule complex with water and/or formaldehyde. This interaction results in a substantial energy barrier (1.86 eV) to fully separate **COM1** to the individual product fragments **P2** (water), **P3** (formaldehyde), and **P4** (vinyl alcohol radical cation). Similarly, separating **COM1** to produce vinyl radical cation, **P4**, and a hydrogen-bridged complex of neutral water and formaldehyde, **COM4**, requires 1.61 eV. Thus, as a result of the strong ion−molecule interaction, the rate-limiting step in the formation of vinyl alcohol radical cation is not the formation of the six-membered proton-transfer transition state (**TS1**), but rather the separation of the product fragments (Table 2). On the other hand, loss of either neutral water (**P2**) or neutral formaldehyde (**P3**) preserves the strong hydrogen-bridged ion−molecule interaction involving the vinyl alcohol radical cation in the product complex (**COM2**, **COM3**, Figure 5). This accounts for the lower appearance energy for water or, alternatively, formaldehyde loss (9.8 ± 0.1 and 9.9 ± 0.1 eV, respectively, Table 2) compared to formation of the vinyl alcohol radical cation (m/z 44, 10.3 ± 0.1 eV, Table 2). Indeed, calculations show that the rate-limiting step in water (or formaldehyde) loss is the transfer of the proton via the six-membered transition state (9.72 eV, Table 2). Water (or formaldehyde) separated fully from the product complex lies at only 9.28 eV (9.26 eV) (Table 2). A mechanism via the common intermediate **COM1** also accounts for the similar appearance energies of formaldehyde and water seen in the experiment (9.8 ± 0.1 and 9.9 ± 0.1 eV, respectively, Table 2). Additionally, the computational prediction of a common intermediate is in accordance with the experimental breakdown diagram presented in Figure 3. Also, since proton transfer occurs between two OH groups, the proposed mechanism via a concerted six-membered-ring transition state and product complex **COM1** matches the observations in the deuterium labeling experiments (Table 2). Furthermore, the computed AEs arising via **COM1** are in excellent agreement with experimental findings. We have computed a variety of other potential channels and find that they exhibit higher barriers and thus can be excluded. A detailed discussion of these mechanisms can be found in the Supporting Information. Finally, this mechanism can account for the absence of water- and formaldehyde-loss peaks in the mass spectrum for glycerol dimer, as will be discussed in more detail in Section 3.3.

The second primary fragmentation channel arises from the elongated, and thus weakened, C−C bond in the relaxed radical cation, which is a common feature in the lowest energy

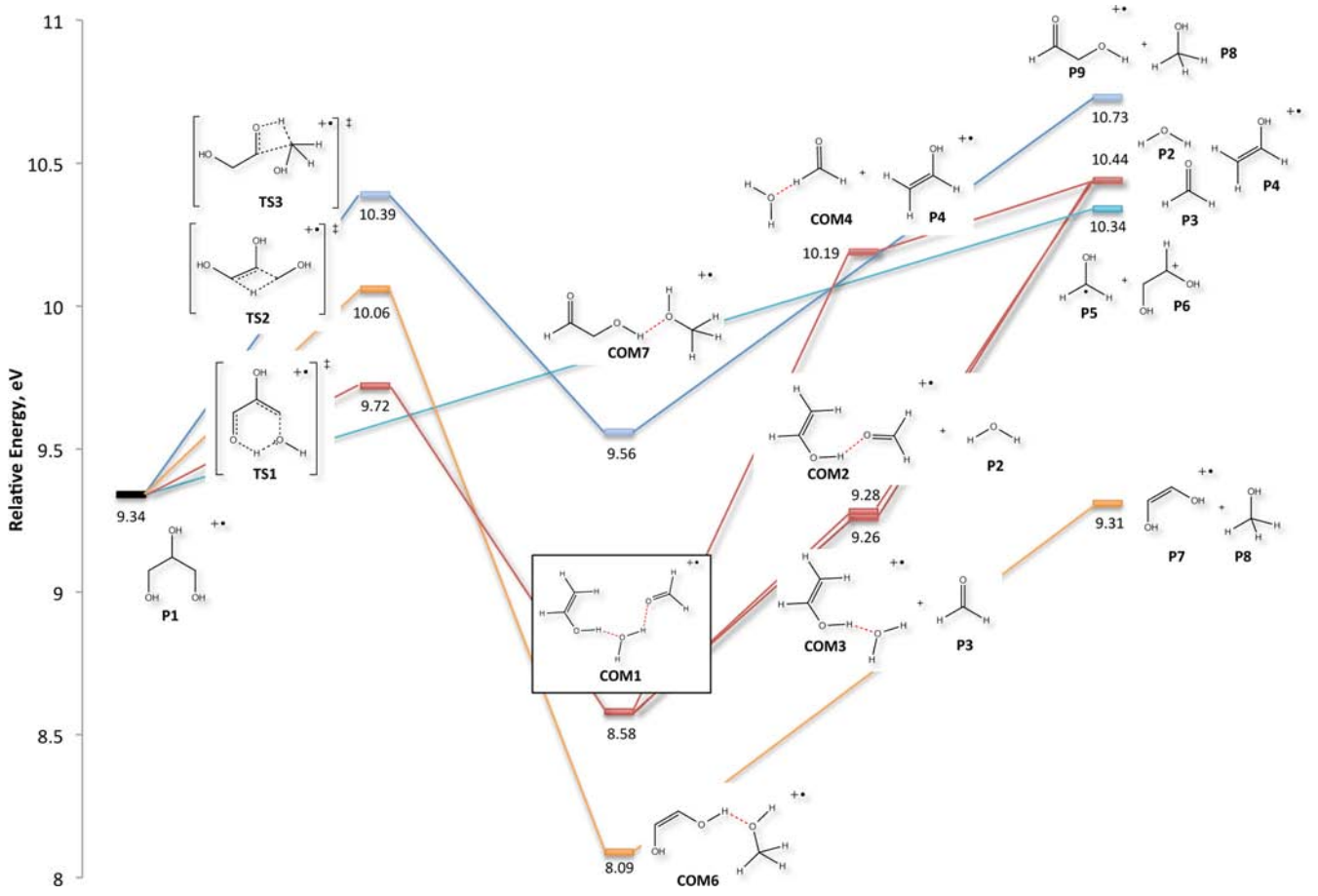

Figure 5. Summary of the main fragmentation pathways. Energies (in eV) calculated at UCCSD(T)/6-31+G(p,d)//ωB97X/6-31+G(p,d). The zero of energy is neutral glycerol (conformer 100). TS: transition state, COM: complex, P: product.

Table 2. Summary of Activation Barriers (in eV) and Deuterium-Labeling Experiments for the Photodissociation of Monomeric Gas-Phase Glycerol[a]

	experiment		
pathway	±0.1	D5-glycerol (*m/z*)	calcd
water loss, *m/z* 74 six-membered, **TS1** prod, **COM1** + **P2**	9.8	$C_3HD_5O_2^+$ (79)	**9.72** 9.28
formald. loss, *m/z* 62 six-membered, **TS1** prod, **COM3** + **P3**	9.9	$C_2D_3H_3O_2^+$ (65) $C_2D_4H_2O_2^+$ (66) *m/z* (65:66) = 8:1	**9.72** 9.26
methanol loss, *m/z* 60 OH abstr, **TS3**		$C_2D_3HO_2^+$ (63)	10.39
CH abstr, **TS2**	10.0	$C_2D_2H_2O_2^+$ (62)	**10.06**
ald prod, **P9**		*m/z* (63:62) = 2:1	10.73
ene-diol prod, **P7**			9.31
m/z 61 prod, **P5** + **P6**	10.3	$C_2D_3H_2O_2^+$ (64)	**10.34**
vinyl alcohol, *m/z* 44 six-membered, **TS1** fully sep prod, **P2** + **P3** + **P4** H_2O-formald COM, **COM4** + **P4**	10.3	$C_2D_3HO^+$ (47)	9.72 10.44 **10.19**

[a]Calculations carried out at UCCSD(T)/6-31+G(p,d)//ωB97X/6-31+G(p,d). Bold: rate-limiting step.

conformers of the ionized glycerol monomer (see Section 3.2). This route can result in methanol (**P8**) loss or the loss of a CH_2OH radical (**P5**) from the parent radical cation (*m/z* 92), accounting for fragments with *m/z* 60 (**P7** or **P9**) and 61 (**P6**), respectively. In the case of the cation with *m/z* 61, loss of a CH_2OH radical does not feature an exit barrier (see IRC in the Supporting Information), as is often observed for a radical mechanism of this type. The fully separated products are predicted to lie at 10.34 eV (Table 2), which is in very good agreement with the experimentally observed appearance energy of 10.3 ± 0.1 eV (Table 2). The proposed mechanism is also in agreement with deuterium labeling experiments, which indicate that three of the five C-D are retained in the product. In the case of fragment with *m/z* 60, we propose two mechanisms, in which the hydrogen atom required to form methanol can either be pulled off the adjacent OH group or the terminal C−H (Figure 5). The former channel yields an aldehyde intermediate (**P9**), whereas the latter yields an ene-diol (**P7**). Deuterium labeling experiments indicate that two products are formed in a ratio of about 2.3:1 (Table 2). The major product features two deuterium atoms suggesting that abstraction of C−H(D) is favored over dissociation of the hydroxylic proton. Indeed, the calculated barrier for C−H abstraction lies lower than that for O−H abstraction and is found to be in very good agreement with the experimentally measured value (10.06 eV, Table 2).

We also analyzed some of the secondary product fragments, such as fragment *m/z* 45. Detailed discussions can be found in the Supporting Information.

3.2.3. Hydrogen-Bridged Ion−Molecule Interactions. Most fragmentation channels studied in this paper involve highly stable hydrogen-bridged ion−molecule intermediate or product complexes. Such complexes have very strong hydrogen bonds due to the presence of the charge, whose nature we now

dx.doi.org/10.1021/ja405511v | J. Am. Chem. Soc. 2013, 135, 14229−14239

investigate. Table 3 lists the hydrogen-bond lengths and EDA terms[40,65] for the binding energy of the molecular species in

Table 3. Hydrogen-Bond Lengths and ALMO Energy Decomposition Analysis Terms and Binding Energies for Selected Complexes and the S22 Water Dimer for ωb97X/6-311++G(2df,2pd) in kcal/mol

complex	FRZ	POL	CT	BIND	R_{HB} (Å)
$(H_2O)_2$	−3.19	−0.92	−1.51	−5.62	1.952
COM2	−4.36	−12.88	−12.17	−26.77	1.487
COM3	−6.19	−10.37	−11.29	−25.80	1.491
COM7	−2.67	−12.32	−12.60	−24.33	1.412

selected complexes with the radical electron located, in all cases, on the species with the most carbon atoms. The EDA for the neutral water dimer (at the S22 geometry)[66] is also shown for comparison. The binding energies for **COM2**, **COM3**, and **COM7** are exceptionally strong, approximately five times larger than that for the hydrogen bond in the water dimer. One notable difference is the increase in the relative importance of polarization (POL) to charge transfer (CT) from ∼60% of the charge-transfer term in the water dimer to very comparable charge transfer and polarization terms in **COM2**, **COM3**, and **COM7**. The increased fraction of polarization is not surprising for charged systems, since conventional wisdom on these hydrogen-bridged ion−molecule interactions is that they are dominated by polarization. However, our calculations show that charge transfer is still equally important, which is a robust conclusion because the ALMO EDA polarization term is an upper bound to the magnitude of true polarization.[67] Equivalently, the magnitude of the ALMO EDA charge-transfer term is a lower bound.

Complementary occupied virtual orbital pair (COVP) analysis[68] in the α and β spaces for the bimolecular complexes **COM2**, **COM3**, and **COM7** shows that charge transfer is almost exclusively to the radical cation species, with negligible back bonding and, moreover, is roughly symmetric with respect to spin. The approximate symmetry with respect to spin is reasonable given that most of the spin density of the unpaired electron resides in the C−C bond, which does not participate in the hydrogen-bridged interaction. The most important COVPs for these interactions in the α space appear in Figure 6 along with the corresponding infinite order perturbation theory charge-transfer energy lowerings. It is clear from Figure 6 that the basic lone pair to σ^* charge-transfer interaction in the water dimer (a) is also present in **COM2** (b), **COM3** (c), and **COM7** (d).

COM1 contains vinyl alcohol radical cation, water, and formaldehyde with two hydrogen-bonding interactions. The EDA terms for the many body expansion of the cluster to third order (which is exact) are shown in Table 4 along with the EDA of the total interaction of the three species. The interaction energy (INT) is the binding energy neglecting geometric distortion. The dominant two-body term is the vinyl alcohol cation interaction with water (E_2[AW]), which shows a fairly even split between charge-transfer and polarization contributions, as was seen above. COVP analysis of this interaction again shows rough spin symmetry for the same reason discussed previously, and it reveals that charge donation is primarily from water to the vinyl alcohol radical cation with minimal back donation. The most significant orbital pair with

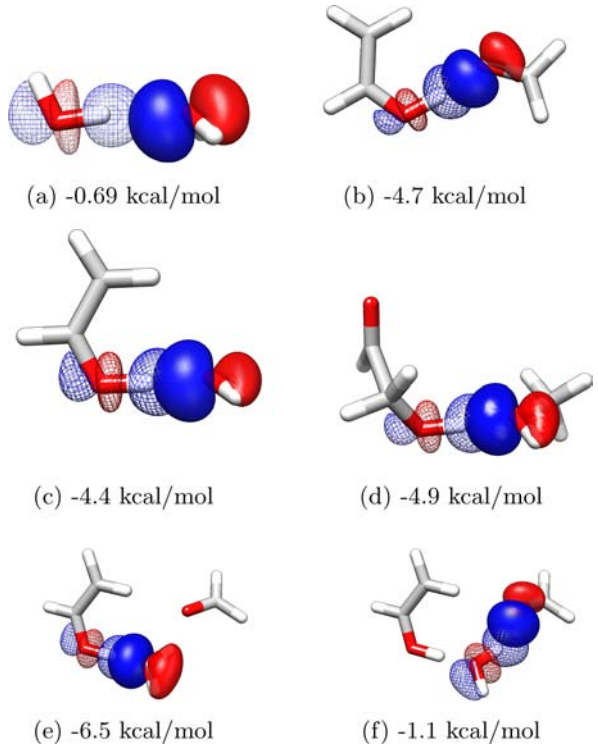

Figure 6. COVPs for (a) the water dimer, (b) **COM2**, (c) **COM3**, (d) **COM7**, (e) **COM1** vinyl alcohol radical cation and water, (f) **COM1** vinyl alcohol radical cation and formaldehyde. The virtual orbital of the pair is depicted as mesh. All orbital pairs and energy lowerings (kcal/mol) are for the α space. The orbitals and corresponding energy lowerings in the beta space are roughly the same (identical for restricted (a) and (f)) because the radical electron is in the C−C bond and does not directly participate in the hydrogen-bridged interactions.

Table 4. Hydrogen-Bond Lengths and ALMO Energy Decomposition Analysis Terms for the Many Body (MB) Expansion of the COM1 Binding Energy for ωb97X/6-311++G(2df,2pd) in kcal/mol[a]

MB term	FRZ	POL	CT	INT	BIND	R_{HB} (Å)
E_2[AW]	2.81	−14.87	−16.45	−28.51	–	1.382
E_2[AF]	−10.33	−2.09	−0.36	−12.78	–	
E_2[WF]	1.47	−1.53	−2.84	−2.91	–	1.750
E_3[AWF]	−0.17	−1.99	−1.24	−3.40	–	
TOT	−6.23	−20.48	−20.89	−47.59	−41.79	

[a]A indicates the vinyl alcohol radical cation, W indicates water, and F indicates formaldehyde. E_2 and E_3 are two- and three-body terms, respectively.

corresponding infinite-order perturbation theory charge-transfer energy lowering is plotted in Figure 6e.

The E_2[AF] term corresponding to the interaction between the vinyl alcohol radical cation and formaldehyde is also quite large but different in character. It is predominantly a frozen (FRZ) orbital interaction with a considerably smaller contribution from polarization and negligible charge transfer. Orbital interactions vanish due to the fairly large intermolecular spacing, and the two-body term is largely described by permanent electrostatic interactions between the charged radical cation and the favorably aligned dipole of formaldehyde. The two-body term arising from the interaction of water with formaldehyde (E_2[WF]) is considerably smaller than the other

dx.doi.org/10.1021/ja405511v | J. Am. Chem. Soc. 2013, 135, 14229−14239

pairwise interactions because only neutral molecules are involved. The EDA reveals a polarization to charge-transfer partitioning reminiscent of the neutral water dimer though with an unfavorable frozen term likely due to the contracted hydrogen-bond distance. The α COVP for this pair interaction appears in Figure 6f and, as expected, resembles that of the neutral water dimer.

The three-body contribution to the **COM1** interaction energy is comparable to that of the water and formaldehyde pair interaction and primarily polarization and charge transfer in origin with negligible frozen contribution due to the pairwise additivity of permanent electrostatics and minimal overlap of frozen occupied orbitals from all three fragments. The non-negligible polarization and charge-transfer terms reflect the fairly large perturbation introduced by a charged species. Analysis of the charge-transfer energy lowering for the three-fragment water **COM1** complex by infinite order perturbation theory (−17.1 kcal/mol) shows that 81% of the energy lowering is due to charge transfer from water to the vinyl alcohol radical cation and 16% is due to charge transfer from formaldehyde to water, and there is again minimal charge transfer between vinyl alcohol cation and formaldehyde. Perhaps most interestingly, the infinite order perturbation theory charge-transfer energy lowering from the three-body term is dominated by fairly equal parts water to vinyl alcohol radical cation and formaldehyde to water charge donation to stabilize the cation.

3.3. Glycerol Dimer. Since glycerol is known to form extensive intermolecular hydrogen-bonding networks,[69−71] we were interested in how the dissociative channels are influenced by the presence of a second glycerol molecule. Moreover, understanding its fragmentation pathways forms the first step in a series of investigations involving increasingly complex polyol compounds in order to elucidate the mechanisms involved in carbohydrate chemistry.

A conformer search for neutral glycerol dimer was carried out (see Section 2.2 for details). The lowest structure is displayed in Figure 7 and lies 0.71 eV (ωB97X/6-311++G(p,d)//B3LYP/6-311++G(p,d)) below two isolated neutral monomeric glycerol molecules (conformer 100). Table 5 summarizes the relative energies and some structural parameters of the lowest 10 dimer conformers. The low-lying structures feature mainly intermolecular rather than intramolecular hydrogen bonds. This is not surprising, as the directionality and distance of intramolecular hydrogen bonds are not as favorable. For the two lowest structures, both intramolecular hydrogen bonds are between the two terminal OH groups, which allows each of the glycerol molecules to adopt a chairlike conformation.

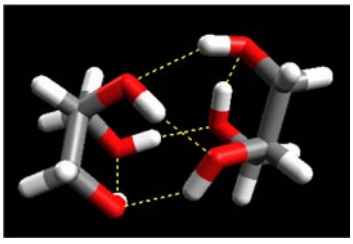

Figure 7. Cartoon of the lowest energy dimer structure (conformer 1), highlighting the hydrogen bonding network.

Upon ionization, almost the entire spin density (Figure 8) is located on one of the glycerol molecules, and so a similar trend in geometric parameters as for monomeric glycerol radical cation is observed, i.e., one of the C−C bonds is extended considerably (to 1.83 Å) (Table 6). The finding that the glycerol dimer radical cation can, to a first approximation, be described as a monomeric glycerol radical cation in the presence of a spectator glycerol, suggests that the dissociative photoionization pathways observed should resemble those of the monomeric species. Indeed, just as for the monomeric radical cation, fragment ions resulting from the loss of m/z 31 (attributed to hydroxymethyl radical) and m/z 48 (assigned to the loss of neutral water and formaldehyde) are observed for the glycerol dimer radical cation (Table 7). Furthermore, proton transfer via a six-membered transition state (analogous to Figure 5) is expected to be very facile due to the hydrogen-bonding network that favors intramolecular hydrogen bonds between the two terminal OH groups. This is supported by the

Table 5. Relative Energies (in kcal/mol) and Key Structural Parameters for the 10 Lowest Energy Gas-Phase Glycerol Dimer Conformers[a]

	relative energy		no. of H-bonds	
	ωB97X	B3LYP	(no. of intra. H-bonds, type)	
conf	/6-311++G(p,d)		<2.0 Å	<2.5 Å
1	0.00	0.00	4 (2, TT)	6 (2, TT)
2	0.09	−0.04	5 (2, TT)	6 (2, TT)
3	1.10	1.45	5 (1, TT)	6 (2, TT, CT)
4	1.11	0.83	5 (1, TT)	6 (2, TT, CT)
5	1.49	1.33	5 (1, TT)	6 (2, TT, CT)
6	1.89	2.02	5 (1, TT)	6 (2, TT, CT)
7	1.96	1.98	5 (1, TT)	6 (2, TT, CT)
8	2.07	2.01	5 (1, TT)	6 (2, TT, CT)
9	2.09	2.02	5 (1, TT)	6 (2, TT, CT)
10	2.44	2.59	5 (1, TT)	6 (2, TT, CT)

[a]Structures were optimized at the B3LYP/6-311++G(p,d) level of theory. The type of hydrogen bond is indicated by TT (between the two terminal OH groups or CT (between a terminal and a central OH group).

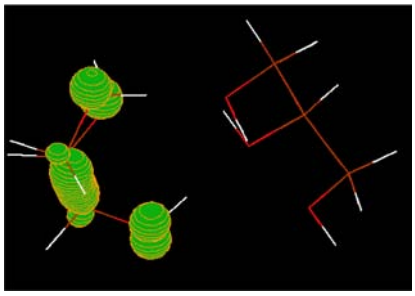

Figure 8. Spin density in glycerol dimer radical cation (cutoff: 0.02).

Table 6. Key Structural Parameters for Gas-Phase Glycerol Dimer Radical Cation, Conformer 1[a]

	C−C		
	long, Å	short, Å	TT O···H, Å
radical cation	1.83	1.53	2.34
neutral	1.53	1.52	1.83

[a]Radical cation indicates the glycerol molecule that displays most of the spin density in the dimer. TT O···H is the hydrogen-bond distance between the two terminal OH groups.

dx.doi.org/10.1021/ja405511v | J. Am. Chem. Soc. 2013, 135, 14229−14239

Table 7. Appearance Energies (AEs) (in eV ±0.1) Measured in the Dissociative Photoionization of Glycerol Between 93 and 185 *m/z* (supersonic beam)

ion (*m/z*)[a]	fragment(s) lost (*m/z*)	AEs (eV)
$[C_3H_8O_3 + H]^+$ (93)	91	10.5
$[C_3H_8O_3 + C_2H_2O]^+$ (135)	49	10.0
$[C_3H_8O_3 + C_2H_3O]^+$ (136)	48	9.7
$[C_3H_8O_3 + C_2H_5O_2]^+$ (153)	31	9.5
$[C_3H_8O_3 + C_3H_9O_3]^+$ (185)	91	9.9

[a]No glycerol dimer cation (*m/z* 184) is detected above the background noise. However, contrary to the parent glycerol monomer cation (*m/z* 92), the photon energy step size was not decreased and the collection time not increased when recording the mass spectrum in the region of *m/z* 184.

appearance energy observed for fragment *m/z* (184−48) = *m/z* 136 (9.6 eV, Table 7), which lies close in energy to the 9.72 eV barrier computed for the concerted six-membered dissociation of monomeric glycerol (Table 2).

However, in contrast to monomeric glycerol, the presence of a spectator glycerol molecule is expected to considerably lower the barrier affiliated with separating the resulting products of this reaction (e.g., water, formaldehyde and the vinyl alcohol radical cation) as it aids the delocalization of positive charge and spin density. This could explain why, contrary to monomeric glycerol, no *m/z* (184−18) (water loss) or *m/z* (184−30) (formaldehyde loss) peaks are observed in the mass spectrum of the glycerol dimer radical cation (Table 7), but rather dissociation into three product fragments occurs. The other main difference to monomeric glycerol radical cation is the presence of M + 1 peaks in the mass spectrum of clustered glycerol species, such as *m/z* 93 and 185. These correspond to protonated monomeric and dimeric glycerol, respectively. We propose that these protonated species occur from $H^\bullet$ transfer within $(glycerol)_n$ radical cation species, followed by dissociation of the cluster into fragments, as follows:

$$[gly_n]^{+\bullet} \rightarrow [gly - H]^\bullet + [gly_{n-1} + H]^+ \quad (2)$$

Here, $[gly - H]^\bullet$ denotes a glycerol molecule from which a hydrogen atom is abstracted.

Although such a process is highly unlikely in an uncharged species (cf. the pK_a value of an OH group in glycerol), ionization makes this process feasible. The products for reaction 2 with $n = 2$, for example, lie at 9.56 eV (ωB97X/6-311++G(p,d)//B3LYP/6-311++G(p,d)) with respect to two neutral isolated glycerol molecules (conformer 100).

Since the AE for the protonated glycerol dimer cation (*m/z* 185) lies above the AEs of fragment ions with *m/z* 153, 136, and 135, this suggests that these photodissociation products arise from the unprotonated glycerol dimer radical cation (*m/z* 184).

4. CONCLUSIONS

In this study, the dissociative photoionization of glycerol and glycerol dimer is investigated both experimentally and theoretically. Low pressure conditions combined with tunable synchrotron radiation and time-of-flight mass spectrometry allow appearance energies of radical species to be determined with high-energy resolution. Glycerol is found to have a very high tendency to fragment upon photoionization, which we find is due to the weakened carbon framework in the glycerol radical cation. Its lowest barrier to rearrangement is a six-membered transition structure leading to a stable ternary intermediate complex (**COM1**) composed of formaldehyde, water, and vinyl alcohol radical cation, with an energy about 0.75 eV below glycerol cation.

Due to the presence of strong hydrogen-bridged ion−molecule interactions, full separation of the three components in **COM1** is energetically unfavorable and explains why either water- or formaldehyde-loss products are observed at lower appearance energies experimentally. We also elucidate detailed mechanisms leading to fragments that are observed at higher energies, such as the loss of methanol and hydroxymethyl radical, and show that these arise as a result of the weakened C−C bond upon ionization.

In several fragmentation channels the observed appearance energy is due to energy cost of separating the product fragments from one another rather than the rearrangements to the product complex. This is because the intermediates exhibit very strong (>25 kcal/mol) hydrogen-bridged ion−molecule interactions. In addition, several product fragments were themselves identified as ion−molecule complexes, involving similarly strong hydrogen-bridged ion−molecule interactions, making such interactions one of the recurring themes in this study. While they have been previously attributed to ion−dipole interactions, we perform an energy decomposition analysis of the complexes, which reveals that about half the interaction energy is associated with charge transfer.

In a first attempt to understand the fragmentation pathways in complex polyols and carbohydrates, we also studied the dissociative photoionization of glycerol dimer. Our studies suggest that the glycerol dimer radical cation can be viewed, to a first approximation, as a monomeric glycerol cation in the presence of a spectator molecule and therefore exhibits similar photodissociation pathways to monomeric glycerol. The main difference is the absence of a water- and formaldehyde-loss peak, which we propose to be due to the spectator glycerol molecule. Its presence causes a lowering in the product dissociation barrier and allows more facile separation of the three fragments. Due to the structural resemblance between glycerol dimer and simple carbohydrates, these results suggest that carbohydrates should exhibit similar rich fragmentation patterns.

The combined use of electronic structure calculations with synchrotron based mass spectrometry promises to be a powerful tool in elucidating the molecular decomposition pathways of systems relevant to energy conversion processes.

■ ASSOCIATED CONTENT

Ⓢ Supporting Information

Supplementary experimental data; glycerol radical cation conformer study; alternative mechanisms. This information is available free of charge via the Internet at http://pubs.acs.org

■ AUTHOR INFORMATION

Corresponding Author

mhg@cchem.berkeley.edu

Author Contributions

[‖]These authors contributed equally.

Notes

The authors declare no competing financial interest.

■ ACKNOWLEDGMENTS

The experiments were carried out at the Advanced Light Source (ALS) at Lawrence Berkeley National Laboratory; the ALS and authors (F.B., A.G., P.R.H., S.R.L., M.A., M.H.G.) are supported by the Office of Science, Office of Basic Energy Sciences, Office of the U.S. Department of Energy under contract no. DE-AC02-05CH11231, through the Chemical Sciences Division.

■ REFERENCES

(1) Remize, F.; Barnavon, L.; Dequin, S. *Metab. Eng.* **2001**, *3*, 301.
(2) Nicolaou, K. C.; Mitchell, H. J. *Angew. Chem., Int. Ed.* **2001**, *40*, 1576.
(3) Bozell, J. J. *Chemicals and Materials from Renewable Resources*; American Chemical Society: Washington, D.C., 2001; Vol. *784*
(4) Ruhal, R.; Aggarwal, S.; Choudhury, B. *Green Chem.* **2011**, *13*, 3492.
(5) Huber, G. W.; Iborra, S.; Corma, A. *Chem. Rev.* **2006**, *106*, 4044−4098.
(6) Paine, J. B., III; Pithawalla, Y. B.; Naworal, J. D. *J. Anal. Appl. Pyrolysis* **2008**, *82*, 10.
(7) Paine, J. B., III; Pithawalla, Y. B.; Naworal, J. D. *J. Anal. Appl. Pyrolysis* **2008**, *82*, 42.
(8) Paine, J. B., III; Pithawalla, Y. B.; Naworal, J. D. *J. Anal. Appl. Pyrolysis* **2008**, *83*, 37.
(9) Stein, Y. S.; Antal, M. J.; Antal; Jones, M. *J. Anal. Appl. Pyrolysis* **1983**, *4*, 283.
(10) Paine, J. B., III; Thomas, C., Jr. *J. Anal. Appl. Pyrolysis* **2007**, *80*, 297.
(11) Nimlos, M.; Blanksby, S.; Qian, X.; Himmel, M. E.; Johnson, D. *J. Phys. Chem. A* **2006**, *110*, 6145.
(12) Sun, W.; Liu, J.; Chu, X.; Zhang, C.; Liu, C. *J. Mol. Struct.: THEOCHEM* **2010**, *942*, 38.
(13) Laino, T.; Tuma, C.; Curioni, A.; Jochnowitz, E.; Stolz, S. *J. Phys. Chem. A* **2011**, *115*, 3592.
(14) Callam, C. S.; Singer, S. J.; Lowary, T. L.; Hadad, C. M. *J. Am. Chem. Soc.* **2001**, *123*, 11743 .
(15) Chelli, R.; Gervasio, F. L.; Gellini, C.; Procacci, P.; Cardini, G.; Schettino, V. *J. Phys. Chem. A* **2000**, *104*, 11220.
(16) Cool, T. A.; Nakajima, K.; Mostefaoui, T. A.; Qi, F.; McIlroy, A.; Westmoreland, P. R.; Law, M. E.; Poisson, L.; Peterka, D. S.; Ahmed, M. *J. Chem. Phys.* **2003**, *119*, 8356.
(17) Cool, T. A.; Nakajima, K.; Taatjes, C. A.; McIlroy, A.; Westmoreland, P. R.; Law, M. E. *Proc. Combust. Inst.* **2005**, *30*, 1681.
(18) Hansen, N.; Klippenstein, C. A.; Taatjes, S. J.; Miller, J. A.; Wang, J.; Cool, T. A.; Yang, B.; Wei, L. X.; Huang, C. Q.; Wang, J.; Qi, F.; Law, M. E.; Westmoreland, P. R. *J. Phys. Chem. A* **2006**, *110*, 3670.
(19) Li, Y.; Qi, F. *Acc. Chem. Res.* **2010**, *43*, 68.
(20) Kohse-Hoeinghaus, K.; Osswald, P.; Cool, T. A.; Kasper, T.; Hansen, N.; Qi, F.; Westbrook, C. K.; Westmoreland, P. R. *Angew. Chem., Int. Ed.* **2010**, *49*, 3572.
(21) Taatjes, C. A.; Hansen, N.; Osborn, D. L.; Kohse-Hoeinghaus, K.; Cool, T. A.; Westmoreland, P. R. *Phys. Chem. Chem. Phys.* **2008**, *10*, 20.
(22) Meot-Ner (Mautner), M. *Chem. Rev.* **2005**, *105*, 213.
(23) Furhmann, C. N.; Daugherty, M. D.; Agard, D. A. *J. Am. Chem. Soc.* **2006**, *128*, 9086.
(24) Das, A.; Mahale, S.; Prashar, V.; Bihani, S.; Ferrer, J.-L.; Hosur, M. V. *J. Am. Chem. Soc.* **2010**, *132*, 6366.
(25) Xu, Z.; Singh, N. J.; Lim, J.; Pan, J.; Kim, H. N.; Park, S.; Kim, K. S.; Yoon, J. *J. Am. Chem. Soc.* **2009**, *131*, 15528.
(26) Payer, D.; Comisso, A.; Dmitriev, A.; Strunskus, T.; Lin, N.; Woell, C.; Devita, A.; Barth, J. V.; Kern, K. *Chem.—Eur. J.* **2007**, *13*, 3900.
(27) Brammer, L.; Swearinger, J. K.; Bruton, E. A.; Sherwood, P. *Proc. Natl. Acad. Sci. U.S.A.* **2002**, *99*, 4956.
(28) Fenniri, H.; Mathivanan, P.; Vidale, K. L.; Sherman, D. M.; Hallenga, K.; Wood, K. V.; Stowell, J. G. *J. Am. Chem. Soc.* **2001**, *123*, 3854.
(29) Krishnamohan-Sharma, C. V.; Clearfield, A. *J. Am. Chem. Soc.* **2000**, *122*, 4394.
(30) Ayotte, P.; Bailey, C. G.; Weddle, G. H.; Johnson, M. A. *J. Phys. Chem. A* **1998**, *102*, 3067.
(31) Castro, M. *J. Phys. Chem. A* **2012**, *116*, 5529.
(32) Prell, J. S.; Williams, E. R. *J. Am. Chem. Soc.* **2009**, *131*, 4110.
(33) Wang, Y.-S.; Chang, H.-C.; Jiang, J.-C.; Lin, S. H.; Lee, Y. T.; Chang, H.-C. *J. Am. Chem. Soc.* **1998**, *120*, 8777.
(34) Terlouw, J. K.; Burgers, P. C. *Encyclopedia of Mass Sepctrometry*; Elsevier:Amsterdam, 2005; Vol. *4*.
(35) Terlouw, J. K.; Heerma, W.; Burgers, P. C.; Holmes, J. L. *Can. J. Chem.* **1984**, *62*, 289.
(36) Sub, D.; Burger, P. C.; Terlouw, J. K. *Rapid Commun. Mass Spectrom.* **1995**, *9*, 862.
(37) Jobst, K. J.; Trikoupis, M. A. *Eur. J. Mass Spectrom.* **2012**, *18*, 183.
(38) Feliks, M.; Ullmann, G. M. *J. Phys. Chem. B* **2012**, *116*, 7076.
(39) Hursak, J.; McGibbon, G. A.; Schwarz, H.; Terlouw, J. K. *Int. J. Mass Spectrom.* **1997**, *160*, 117.
(40) Horn, P. R.; Sundstrom, E. J.; Baker, T. A.; Head-Gordon, M. *J. Chem. Phys.* **2013**, *138*, 134119.
(41) Nicolas, C.; Shu, J. N.; Peterka, D. S.; Hochlaf, M.; Poisson, L.; Leone, S. R.; Ahmed, M. *J. Am. Chem. Soc.* **2006**, *128*, 220.
(42) Kostko, O.; Belau, L.; Wilson, K. R.; Ahmed, M. *J. Phys. Chem. A* **2008**, *112*, 9555.
(43) Belau, L.; Wilson, K. R.; Leone, S. R.; Ahmed, M. *J. Phys. Chem. A* **2007**, *111*, 7562.
(44) Shao, Y.; et al. *Phys. Chem. Chem. Phys.* **2006**, *8*, 3172.
(45) Becke, A. D. *J. Chem. Phys.* **1993**, *98*, 1372.
(46) Møller, C.; Plesset, M. S. *Phys. Rev.* **1934**, *46*, 618.
(47) Chai, J.-D.; Head-Gordon, M. *J. Chem. Phys.* **2009**, *131*, 174105.
(48) Halkier, A.; Helgaker, T.; Jørgensen, P.; Klopper, W.; Koch, H.; Olsen, J.; Wilson, A. K. *Chem. Phys. Lett.* **1998**, *286*, 243.
(49) Raghavachari, K.; Trucks, G. W.; Pople, J. A.; Head-Gordon, M. *Chem. Phys. Lett.* **1989**, *157*, 479.
(50) Urban, M.; Noga, J.; Cole, S. J.; Bartlett, R. J. *J. Chem. Phys.* **1985**, *83*, 4041.
(51) Behn, A.; Zimmerman, P. M.; Bell, A. T.; Head-Gordon, M. *J. Chem. Phys.* **2011**, *135*, 224108.
(52) Fukui, K.; Kato, S.; Fujimoto, H. *J. Am. Chem. Soc.* **1975**, *97*, 1.
(53) Perdew, J. P.; Zunger, A. *Phys. Rev. B* **1981**, *23*, 5048.
(54) Chai, J.-D.; Head-Gordon, M. *J. Chem. Phys.* **2009**, *131*, 174105.
(55) Xu, X.; Alecu, I. M.; Truhlar, D. G. *J. Chem. Theory Comput.* **2011**, *7*, 1667.
(56) *Spartan08*; Wavefunction Inc.: Irvine, CA.
(57) Halgren, T. A. *J. Comput. Chem.* **1996**, *17*, 490.
(58) Wilson, K. R.; Belau, L.; Nicolas, C.; Jimenez-Cruz, M.; Leone, S. R.; Ahmed, M. *Int. J. Mass Spectrom.* **2006**, *155*, 249.
(59) Traeger, J. C.; Kompe, B. W. *Int. J. Mass Spectrom. Ion Processes* **1990**, *101*, 111.
(60) Gauld, J. W.; Radom, L. *Chem. Phys. Lett.* **1997**, *275*, 28.
(61) Ghosh, D.; Golan, A.; Takahashi, L. K.; Krylov, A. I.; Ahmed, M. *J. Phys. Chem. Lett.* **2012**, *3*, 97.
(62) Bellville, D. J.; Bauld, N. L. *J. Am. Chem. Soc.* **1982**, *104*, 5700.
(63) Bellville, D. J.; Pabon, R. A.; Bauld, N. L. *J. Am. Chem. Soc.* **1985**, *107*, 4978.
(64) Sulzbach, H. M.; Graham, D.; Stephens, J. C.; Schaefer, H. F., III *Acta Chem. Scand.* **1997**, *51*, 547.
(65) Khaliullin, R. Z.; Cobar, E.; Lochan, R.; Bell, A. T.; Head-Gordon, M. *J. Phys. Chem. A* **2007**, *111*, 8753.
(66) Jurecka, P.; Sponer, J.; Cerny, J.; Hobza, P. *Phys. Chem. Chem. Phys.* **2006**, *8*, 1985.
(67) Azar, R.; Horn, P. R.; Sundstrom, E. J.; Head-Gordon, M. *J. Chem. Phys.* **2013**, *138*, 084102.
(68) Khaliullin, R. Z.; Bell, A. T.; Head-Gordon, M. *J. Chem. Phys.* **2008**, *128*, 184112.

(69) Chelli, R.; Procacci, P.; Cardini, G.; Califano, S. *Phys. Chem. Chem. Phys.* **1999**, *1*, 879.
(70) Champeney, D.; Joarder, R.; Dore, J. *Mol. Phys.* **1986**, *58*, 337.
(71) Bohmer, R.; Hinze, G. *J. Chem. Phys.* **1998**, *109*, 241.